PCCP

PAPER

Cite this: *Phys. Chem. Chem. Phys.*, 2018, **20**, 20622

Structural and bonding properties of $Cu_3O_3^-$ and $Cu_3O_4^-$ clusters: anion photoelectron spectroscopy and density functional calculations†

Xi-Ling Xu,[a] Bin Yang,[a] Zhi-You Wei,[a] Guo-Jin Cao,[b] Hong-Guang Xu[a] and Wei-Jun Zheng *[ac]

Received 24th May 2018,
Accepted 22nd July 2018

DOI: 10.1039/c8cp03302a

rsc.li/pccp

The structural and electronic properties of $Cu_3O_3^-$ and $Cu_3O_4^-$ were investigated using mass-selected anion photoelectron spectroscopy in combination with density functional theoretical calculations. The vertical detachment energies of $Cu_3O_3^-$ and $Cu_3O_4^-$ were measured to be 3.48 ± 0.08 and 3.54 ± 0.08 eV, respectively. Their geometrical structures were determined by comparison of the theoretical calculations with the experimental results. The most stable structure of $Cu_3O_3^-$ can be characterized as a C_{3v} symmetric six-membered ring structure with alternating Cu–O bonds, in which the plane of the three O atoms is slightly above that of the three Cu atoms. The most stable structure of $Cu_3O_4^-$ can be viewed as a C_s symmetric seven-membered ring with a peroxo unit. The bond order and molecular orbital analyses indicate that the Cu–Cu interactions in $Cu_3O_3^-$ and $Cu_3O_4^-$ are weak. The calculated NICS(0) and NICS(1) values of $Cu_3O_3^-$ are −25.0 ppm and −19.2 ppm, respectively, and those of $Cu_3O_4^-$ are −18.6 ppm and −10.5 ppm, respectively, indicating that they both are significantly aromatic.

1. Introduction

Transition metal oxides have important applications in catalyst systems, biochemical processes, sensors, and electrode materials.[1–5] Many experimental and theoretical studies were conducted to investigate the structures and properties of transition metal oxides.[6–19] Copper oxides such as cuprous oxide (Cu_2O) and cupric oxide (CuO) were widely used as pigments. They are also p-type metal oxide semiconductors and have applications in optics and dry cell batteries.[20] The photoelectron spectrum of CuO^- has been studied by Lineberger and coworkers.[21] The photoelectron spectra of CuO_n^- (n = 1–6)[22,23] and $Cu_2O_n^-$ (n = 1–4)[24] were investigated by Wang and coworkers. The structures and properties of $CuO_4^{-/0}$, CuO_5 and CuO_6 were investigated using matrix isolation infrared spectra and quantum chemical calculations.[25,26] CuO_4 was characterized to be a side-on bonding copper disuperoxide structure $Cu(\eta^2\text{-}O_2)_2$, CuO_5 a superoxo copper ozonide structure $Cu(\eta^2\text{-}O_2)(\eta^2\text{-}O_3)$ and CuO_6 a mononuclear copper dioxygen structure $Cu(\eta^2\text{-}O_2)(\eta^1\text{-}O_2)_2$. Several theoretical studies have been performed to investigate the structures of neutral and charged CuO_n (n = 1–6) clusters.[27–31] The structures and low-lying excited states of Cu_2O_n (n = 1–4) as well as the structures of their anionic and cationic counterparts were also investigated with density functional theory calculations.[32] The ground state structures of $Cu_2O_n^{\pm/0}$ (n = 1–4) are found to exhibit linear or near linear structures. The structure and properties of oxo, peroxo and superoxo isomers of copper oxides and other 3d-metal oxides were investigated with density functional theory calculations by Jena and coworkers.[33,34] Orms and Krylov reported a detailed study on the low-lying electron-detachment and excited states of CuO^-, CuO_2^- and Cu_2O^- anions and on modeling of their photoelectron spectra using equation-of-motion coupled-cluster (EOM-CC) methods.[35]

The investigations of copper oxides mentioned above were mainly focused on one or two copper atoms species. There are a few investigations on Cu_nO_m ($n > 2$) clusters. The structures and electronic properties of Cu_nO_n (n = 1–8) and $Cu_3O_n^{\pm/0}$ (n = 1–6) were studied by theoretical calculations.[36,37] The magnetic properties of seven larger Cu_nO_m clusters with $n \geq 4$ were investigated using first principles by Yang *et al.*[38] The results suggested the oxygen-rich clusters (Cu_4O_5, $Cu_{16}O_{15}$, and $Cu_{28}O_{27}$) to be magnetic. The theoretical calculations of Jadraque and Martín indicated that $Cu_nO_m^{-/0}$ clusters with even and odd number of copper atoms can be represented as $(Cu_2O)_n^+$ and $[(Cu_2O)_nCu]^+$, respectively.[39] The studies of the gas-phase $Cu_nO_m^+$ (n = 3–7; $m \leq 5$) clusters provide insight into the

[a] *Beijing National Laboratory for Molecular Sciences (BNLMS), State Key Laboratory of Molecular Reaction Dynamics, Institute of Chemistry, Chinese Academy of Sciences, Beijing 100190, China. E-mail: zhengwj@iccas.ac.cn; Fax: +86 10 62563167; Tel: +86 10 62635054*

[b] *Institute of Molecular Science, Shanxi University, Taiyuan 030006, China*

[c] *University of Chinese Academy of Sciences, Beijing 100049, China*

† Electronic supplementary information (ESI) available. See DOI: 10.1039/c8cp03302a

essentials of selective catalytic oxidation of NH_3 to N_2 and H_2O on the copper-based catalysts.[40] Very recently, a variety of studies suggested trinuclear copper-oxo core ($[Cu_3(\mu\text{-}O)_3]^{2+}$) in mordenite zeolite to be the active site for catalyzed oxidation of methane to methanol.[41–43] Although there were a number of theoretical calculations on trinuclear copper oxides,[36,37] there is no report on photoelectron experimental study of these oxides. Considering the importance of trinuclear copper oxides in catalysis and the lack of photoelectron data, in this work, we investigated the structural and bonding properties of $Cu_3O_3^-$ and $Cu_3O_4^-$ clusters using mass-selected anion photoelectron spectroscopy and density functional theory calculations.

2. Experimental and theoretical methods

2.1. Experimental methods

The experiments were conducted on a home-made apparatus consisting of a laser vaporization source, a time-of-flight (TOF) mass spectrometer and a magnetic-bottle photoelectron spectrometer, which has been described in detail previously.[44] In brief, the $Cu_3O_3^-$ and $Cu_3O_4^-$ cluster anions were generated in the laser vaporization source by laser ablation of a rotating and translating copper target with the second harmonic (532 nm) light pulses of a Nd:YAG laser (Continuum Surelite II-10). Helium gas with $\sim$4 atm backing pressure was allowed to expand through a pulsed valve over the target. The residual oxygen in the carrier gas and on the target surface is enough for generating $Cu_3O_3^-$ and $Cu_3O_4^-$ clusters. The generated cluster anions were mass-analyzed by the TOF mass spectrometer. The $Cu_3O_3^-$ and $Cu_3O_4^-$ clusters were each mass-selected by a mass gate and decelerated by a momentum decelerator before being photodetached with the 266 nm laser beam from a second Nd:YAG laser. The photodetached electrons were energy-analyzed by the magnetic-bottle photoelectron spectrometer. The photoelectron spectra were calibrated using the spectra of Cu^- and Au^- taken at similar conditions. The resolution of the photoelectron spectrometer was approximately 40 meV for electrons with 1 eV kinetic energy.

2.2. Theoretical methods

The theoretical calculations were performed using density functional theory with the Becke's three-parameter and Lee–Yang–Parr's gradient corrected correlation hybrid functional (B3LYP),[45,46] as implemented in the Gaussian 09 program package.[47] The aug-cc-pVTZ basis set[48] was used for the O atoms, and the aug-cc-pVTZ-pp basis set[49] was used for the Cu atoms. The B3LYP functional has been shown to be suitable for copper oxide clusters in previous reports.[25,36,37,50] To further confirm the reliability of the B3LYP functional, we also calculated the relative energies and vertical detachment energies (VDEs) of $Cu_3O_3^-$ using the PBE0 and B3P86 functionals with the same basis sets. The relative stabilities of three isomers of $Cu_3O_3^-$ at three functionals are same and the calculated VDE of isomer 3A from the B3LYP functional is in better agreement with the experimental value than those from the PBE0 and B3P86 functionals (see Table S1 in the ESI†). Therefore, we adopt the B3LYP functional for the calculations in this work. We have considered many initial structures including different spin multiplicities during the calculations. All the geometry optimizations were conducted without any symmetry constraint. Harmonic vibrational frequencies were calculated at the same level of theory to make sure that the optimized structures correspond to true local minima. The zero-point vibrational energy corrections were included for the relative energies of isomers. The theoretical vertical detachment energy (VDE) was calculated as the energy difference between the neutral and anion at the geometry of the anionic species. The theoretical adiabatic detachment energy (ADE) was obtained as the energy difference between the neutral and anion with the neutral relaxed to the nearest local minimum using the geometry of the corresponding anion as initial structure. The Wiberg bond order analyses of $Cu_3O_3^-$ and $Cu_3O_4^-$ were conducted with natural bond orbital (NBO) version 3.1 program[51] implemented in the Gaussian 09 package. We also calculated the Mayer bond order and analyzed the orbital compositions by using the natural atomic orbital method with the Multiwfn program.[52]

3. Results and discussion

The photoelectron spectra of $Cu_3O_3^-$ and $Cu_3O_4^-$ obtained with 266 nm photons are shown in Fig. 1. The ADEs and VDEs of $Cu_3O_{3-4}^-$ cluster anions measured from their photoelectron spectra are listed in Table 1. The VDE of each cluster was taken from the maximum of the first peak in its spectrum. The ADE of each cluster was determined by adding the value of instrumental resolution to the onset of the first peak in its spectrum. The optimized geometries of the typical low-lying isomers of $Cu_3O_{3-4}^-$ anions are displayed in Fig. 2 with the most stable structures on the left. The most stable structures of $Cu_3O_{3-4}^-$ anions and their corresponding neutral species viewed from different angles are showed in Fig. 3 and Fig. S1 (in the ESI†). The Cartesian coordinates of the low-lying isomers of $Cu_3O_{3-4}^-$ anions are available in the ESI† (see Table S2). The symmetries, relative energies, and calculated ADEs and VDEs of these low-lying isomers are summarized in Table 1, along with the experimental ADEs and VDEs for comparison. We have also simulated the photoelectron spectra of the low-lying isomers of $Cu_3O_{3-4}^-$ anions based on the theoretically generalized Koopmans' theorem (GKT)[53,54] and compared the simulated spectra with the experimental results in Fig. 1. The simulated spectra are called as density of states (DOS) spectra for convenience. In the DOS spectra, the peak of each transition corresponds to the removal of an electron from an individual molecular orbital of the cluster anion. We set the first peak associated with the HOMO to the position of calculated VDE of each isomer, and then shifted the other peaks associated with the deeper orbitals according to their relative energies compared to the HOMO. The simulated spectra were obtained by fitting the distribution of the transition lines with unit-area Gaussian functions of 0.1 eV width, and the intensities for transitions

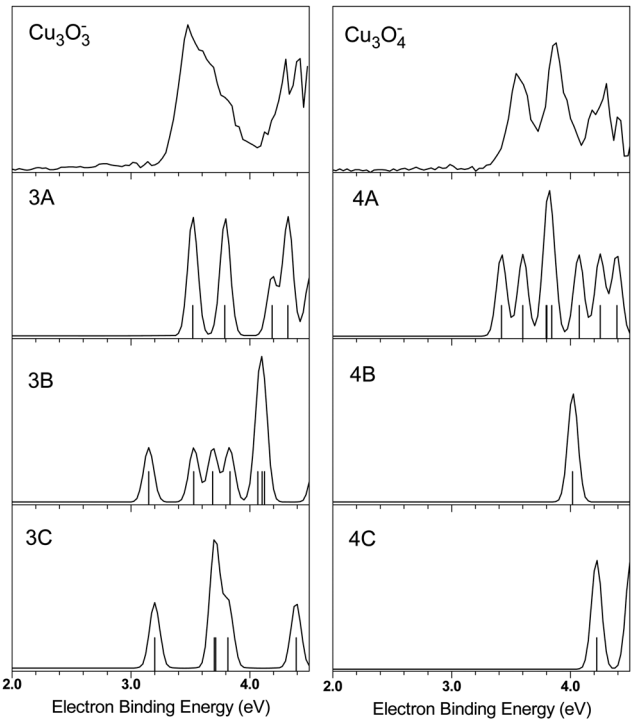

Fig. 1 Comparison between the experimental photoelectron spectra and the simulated DOS spectra of the low-lying isomers of $Cu_3O_3^-$ and $Cu_3O_4^-$. The simulated spectra were obtained by fitting the distribution of the transition lines with unit-area Gaussian functions of 0.1 eV full width at half maximum (FWHM). The vertical lines are the theoretical simulated spectral lines of $Cu_3O_3^-$ and $Cu_3O_4^-$ clusters.

Table 1 Relative energies, ADEs and VDEs of the low-lying structures of $Cu_3O_3^-$ and $Cu_3O_4^-$ calculated at the B3LYP/aug-cc-pVTZ/O/aug-cc-pVTZ-pp/Cu level along with the experimental ADEs and VDEs determined from their photoelectron spectra

				VDE (eV)		ADE (eV)	
	State	Sym.	ΔE (eV)	Theo.	Expt.[a]	Theo.	Expt.[a]
$Cu_3O_3^-$	$^3A_1$	C_{3v}	0.00	3.52	3.48	3.27	3.31
	$^3B_1$	C_{2v}	0.38	3.15		2.89	
	$^1A_1$	C_{2v}	0.82	3.20		3.11	
$Cu_3O_4^-$	$^3A'$	C_s	0.00	3.42	3.54	3.34	3.42
	$^5\Sigma$	$D_{\infty h}$	0.16	4.02		3.99	
	^3A	C_1	0.85	4.22		3.91	

[a] The uncertainties of the experimental values are ± 0.08 eV.

originated from photodetachment of an electron with α or β spin are assumed as same. The relative intensity and width of the simulated bands are due to the overlapping of multiple transitions.

$Cu_3O_3^-$ and Cu_3O_3

As shown in Fig. 1, the experimental photoelectron spectrum of $Cu_3O_3^-$ has a broad band centered at 3.48 eV with a few shoulders in the range of 3.5–4.0 eV, followed by two resolved peaks centered at 4.30 and 4.41 eV. Our theoretical calculations found that the most stable structure (isomer 3A) of $Cu_3O_3^-$ is in $^3A_1$ electronic state. It is a C_{3v} symmetric six-membered ring

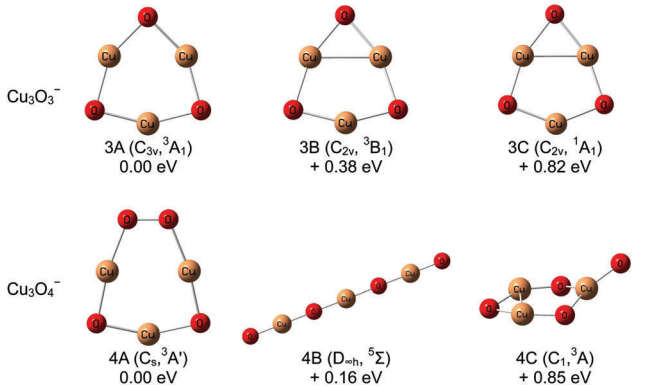

Fig. 2 Geometries of the low-lying isomers of $Cu_3O_3^-$ and $Cu_3O_4^-$ optimized at the B3LYP/aug-cc-pVTZ/O/aug-cc-pVTZ-pp/Cu level of theory.

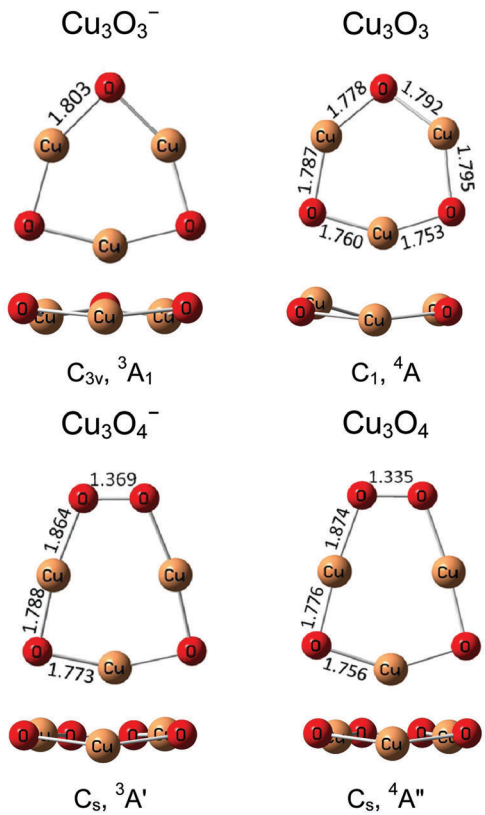

Fig. 3 The most stable structures of $Cu_3O_3^{-/0}$ and $Cu_3O_4^{-/0}$ clusters viewed from different angles. The bond lengths are in angstroms.

with alternating Cu–O bonds, in which the plane of the three O atoms is slightly above that of the three Cu atoms. The bond lengths of Cu–O are 1.803 Å. The calculated VDE of isomer 3A is 3.52 eV, which is in good agreement with the experimental measurement (3.48 eV). The simulated DOS spectrum of isomer 3A is in reasonable agreement with the observed photoelectron spectrum bands (Fig. 1), although the relative intensities of the experimental peaks have not been reproduced by theory. The first and second peaks in the DOS spectrum are consistent with the broad band centered at 3.48 eV and the shoulders in the

experimental spectrum, while the third and fourth peaks in the DOS spectrum are in good agreement with the experimental peaks at 4.30 and 4.41 eV. Based on the DOS spectrum of isomer 3A, those shoulders may be attributed to the low-lying electronic states and vibrational progressions of neutral Cu_3O_3. Isomers 3B and 3C both have C_{2v} symmetry with a five-membered ring Cu_3O_2 and an isosceles triangle Cu_2O sharing a Cu–Cu bond. They are in $^3B_1$ and $^1A_1$ electronic states, respectively. The energies of isomers 3B and 3C are higher than that of isomer 3A by 0.38 and 0.82 eV, respectively, and their theoretical VDEs (3.15 and 3.20 eV) are very different from the experimental value. The simulated DOS spectra of isomers 3B and 3C are very different from the experimental spectrum. Therefore, the existences of isomers 3B and 3C can be excluded. Isomer 3A is the most probable one detected in our experiments. For neutral Cu_3O_3, the most stable structure is slightly different from that of the anion. It is a distorted six-membered ring with alternating Cu–O bonds in ^4A electronic state, in which the plane of the three O atoms intersects with that of the three Cu atoms (Fig. 3). The Cu–O bond lengths in neutral Cu_3O_3 are in the range of 1.753–1.795 Å, slightly shorter than those in the anion.

$Cu_3O_4^-$ and Cu_3O_4

The experimental photoelectron spectrum of $Cu_3O_4^-$ displays two bands centered at 3.54, and 3.88 eV, followed by three overlapping peaks at 4.18, 4.30, and 4.39 eV, respectively. Our theoretical calculations show that the most stable isomer (4A) of $Cu_3O_4^-$ is in $^3A'$ electronic state. It is a C_s symmetric seven-membered ring structure with one O_2 unit, in which the Cu atom locating opposite from the O_2 unit is below the plane formed by the remaining six atoms. The bond length of O–O is 1.369 Å, which is longer than that of O_2 molecule (1.209 Å) and shorter than that of H_2O_2 (1.475 Å), which may also be considered as a peroxo group (will confirmed by the bond order analysis). The bond lengths of Cu–O are in the range of 1.773–1.864 Å. The VDE of isomer 4A is calculated to be 3.42 eV, consistent with the experimental value (3.54 eV). The simulated DOS spectrum of isomer 4A fits the experimental spectrum fairly well (Fig. 1). The first and second peaks in the DOS spectrum are consistent with the peak centered at 3.54 eV, and the highest peak at the center is in agreement with the highest experimental peak at 3.88 eV, whereas the last three peaks in the DOS spectrum are in good agreement with the experimental peaks at 4.18, 4.30, and 4.39 eV, although the positions of the simulated peaks are slightly off from the experimental ones and the relative intensities of the experimental peaks have not been reproduced by theory. Isomer 4B is a linear structure with alternating O–Cu bonds. Isomer 4C can be viewed as an additional O atom interacting with one of three Cu atoms of isomer 3B. The existence of isomer 4B can be excluded because it is higher in energy than isomer 4A by 0.16 eV and its simulated DOS spectrum is very different from the experimental spectrum. Isomer 4C cannot exist in our experiments because it is much higher in energy than isomer 4A by 0.82 eV. Thus, we suggest isomer 4A to be the most probable structure detected in the experiments. The most stable structure of neutral Cu_3O_4 is slightly different from that of the corresponding anion. It is a distorted seven-membered ring with one O_2 unit (Fig. 3). The Cu–O bond lengths attaching the O_2 unit in neutral Cu_3O_4 are 1.874 Å, longer than those (1.864 Å) in the anion, whereas the other Cu–O bond lengths are 1.756 and 1.776 Å, shorter than those (1.773 and 1.788 Å) in the anion. The O–O bond length is 1.335 Å, shorter than that (1.369 Å) in the anion.

The Cu–Cu distances in the most stable isomers of $Cu_3O_3^{-/0}$ are in the range of 2.525–2.824 Å, and those of $Cu_3O_4^{-/0}$ are in the range of 2.523–2.670 Å, longer than the calculated Cu–Cu bond in Cu_2^- (2.34 Å) and Cu_3^- clusters (2.30 Å),[55] indicating that the Cu–Cu interactions are weak in $Cu_3O_3^{-/0}$ and $Cu_3O_4^{-/0}$. To further investigate the chemical bonding in $Cu_3O_3^{-/0}$ and $Cu_3O_4^{-/0}$ clusters, we conducted the Wiberg bond order and Mayer bond order analyses, which are summarized in Table 2. The Cu–Cu Wiberg bond order and Mayer bond order of $Cu_3O_3^-$ are calculated to be 0.16 and 0.11, respectively. Those of Cu_3O_3 are 0.11 and 0.09, respectively. The Cu–Cu Wiberg bond order and Mayer bond order of $Cu_3O_4^-$ are calculated to be 0.15 and 0.14, respectively. Those of Cu_3O_4 are 0.28 and 0.27, respectively. These results imply that the Cu–Cu interactions in these clusters are weak. The Cu–Cu interactions in $Cu_3O_3^-$ are slightly stronger than those in Cu_3O_3, whereas the Cu–Cu interactions in $Cu_3O_4^-$ are slightly weaker than those in Cu_3O_4. The previous studies suggested that the M–M interactions in Fe_3O_3, Co_3O_3, and Ni_3O_3,[16] as well as $Ta_3O_3^-$ [56] are quite strong. Here, the Cu–Cu interactions in $Cu_3O_3^{-/0}$ and $Cu_3O_4^{-/0}$ are weak because the 3d orbitals of Cu atom are fully occupied and the 4s orbitals of Cu atoms mainly interact with the 2p obitals of O atoms.

The bond order analysis shows that the Cu–O Wiberg bond order and Mayer bond order of $Cu_3O_3^-$ are 0.60 and 0.77, respectively. Those of Cu_3O_3 are 0.69 and 0.90, respectively. The Cu–O Wiberg bond order and Mayer bond order of $Cu_3O_4^-$ are 0.67 and 0.88, respectively. Those of Cu_3O_4 are 0.70 and 0.89, respectively. These results suggest that the Cu–O bonds in these clusters are mainly single bonds. The Cu–O bonds in the anions are slightly weaker than those in their neutral counterparts. The O–O Mayer bond orders of $Cu_3O_4^-$ and Cu_3O_4 are 0.77 and 0.84, respectively, suggesting the O_2 unit can be viewed as a peroxo group.

We also analyzed the molecular orbitals of the most stable isomers of $Cu_3O_3^-$ and $Cu_3O_4^-$ and displayed them in Fig. 4. The singly occupied molecular orbital (SOMO) and the highest occupied molecular orbitals (HOMO−3 and HOMO−4) of

Table 2 Maximum Cu–O, Cu–Cu, and O–O bond orders of the most stable structures of $Cu_3O_3^{-/0}$ and $Cu_3O_4^{-/0}$

	Wiberg bond index			Mayer bond index		
	Cu–O	Cu–Cu	O–O	Cu–O	Cu–Cu	O–O
$Cu_3O_3^-$	0.60	0.16	—	0.77	0.11	—
$Cu_3O_4^-$	0.67	0.15	1.33	0.88	0.14	0.77
Cu_3O_3	0.69	0.11	—	0.90	0.09	—
Cu_3O_4	0.70	0.28	1.45	0.89	0.27	0.84

$Cu_3O_3^-$ are mainly composed of the 3d and 4s orbitals of the three Cu atoms and the 2p orbitals of the three O atoms. The SOMO−1, HOMO−2 and HOMO−5 of $Cu_3O_3^-$ are mainly composed of the 3d orbitals of the Cu4 atom, the 3d and 4s orbitals of the other two Cu atoms and the 2p orbitals of the three O atoms. For $Cu_3O_4^-$, the SOMO and SOMO−1 mainly consist of the 3d orbitals of the Cu2 atom, the 3d and 4s orbitals of the other two Cu atoms and the 2p orbitals of the four O atoms, whereas the HOMO−1 mainly consists of the 3d and 4s orbitals of the three Cu atoms and the 2p orbitals of the four O atoms. From the diagrams of the molecular orbitals, one can see that there are barely any overlap between the 3d orbitals of the three Cu atoms, confirming that the Cu–Cu interactions are weak.

The constant electronic charge densities of the most stable isomers of $Cu_3O_3^-$ and $Cu_3O_4^-$ were also analyzed and were showed in Fig. 5. It can be seen from Fig. 5, for constant charge density surface of 0.02 a.u., the electronic charges are distributed uniformly over the Cu–O and O–O bonds, whereas those at the center are very low. For constant charge density surface of 0.04 a.u., the electronic charges are mainly localized on the Cu–O and O–O bonds. For constant charge density surface of 0.12 a.u., the electronic charges are mainly focused on the Cu atoms and the O atoms. These results indicate that the Cu–Cu interactions in $Cu_3O_3^-$ and $Cu_3O_4^-$ are weak, in agreement

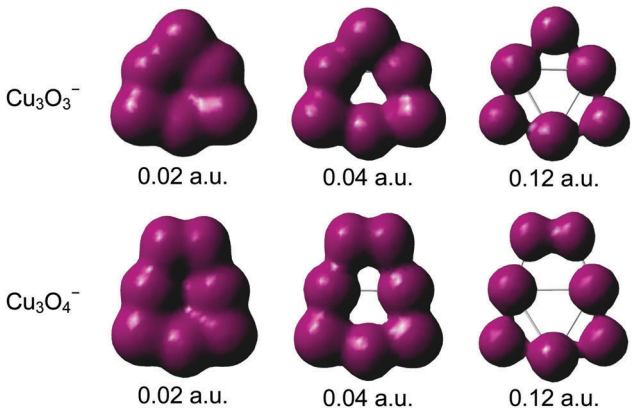

Fig. 5 Constant electronic charge density surfaces of $Cu_3O_3^-$ and $Cu_3O_4^-$ anions at different charge density.

with the calculated Wiberg bond orders of Cu–O (0.60, 0.67) > Cu–Cu (0.16, 0.15). The weak interactions between the three Cu atoms in $Cu_3O_3^-$ and $Cu_3O_4^-$ are also consistent with the long Cu–Cu distances (2.525–2.670 Å) and the molecular orbitals of $Cu_3O_3^-$ and $Cu_3O_4^-$.

Nucleus-independent chemical shifts (NICS) proposed by Schleyer *et al.* can be used to determine the aromaticity of various ring-shaped delocalized electron compounds,[57,58] for example, C_4H_5N (−15.1),[57] C_4H_4O (−12.3),[57] C_6H_6 (−8.9),[58] and $C_5H_5^-$ (−15.0).[58] In general, the more negative the NICS values, the stronger the aromaticity. The original NICS index (termed $NICS(0)_{iso}$) was based on the total isotropic shielding (average shielding) computed at the ring centers, however, $NICS(0)_{iso}$ is non-zero for some nonaromatic rings due to some local effects.[59] Consequently, isotropic NICS(1) value computed at points 1 Å above the ring centers where these local contributions fall off rapidly, was recommended.[59–61] We calculated the NICS(0) and NICS(1) values of the most stable isomers of $Cu_3O_3^-$ and $Cu_3O_4^-$ at the B3LYP/aug-cc-pVTZ/O/aug-cc-pVTZ-pp/Cu level of theory using the Gaussian 09 program package. The NICS(0) and NICS(1) values of $Cu_3O_3^-$ are calculated to be −25.0 ppm and −19.2 ppm, respectively. The NICS(0) and NICS(1) values of $Cu_3O_4^-$ are calculated to be −18.6 ppm and −10.5 ppm, respectively. These large negative NICS values indicate that the $Cu_3O_3^-$ and $Cu_3O_4^-$ clusters both exhibit significant aromaticity.

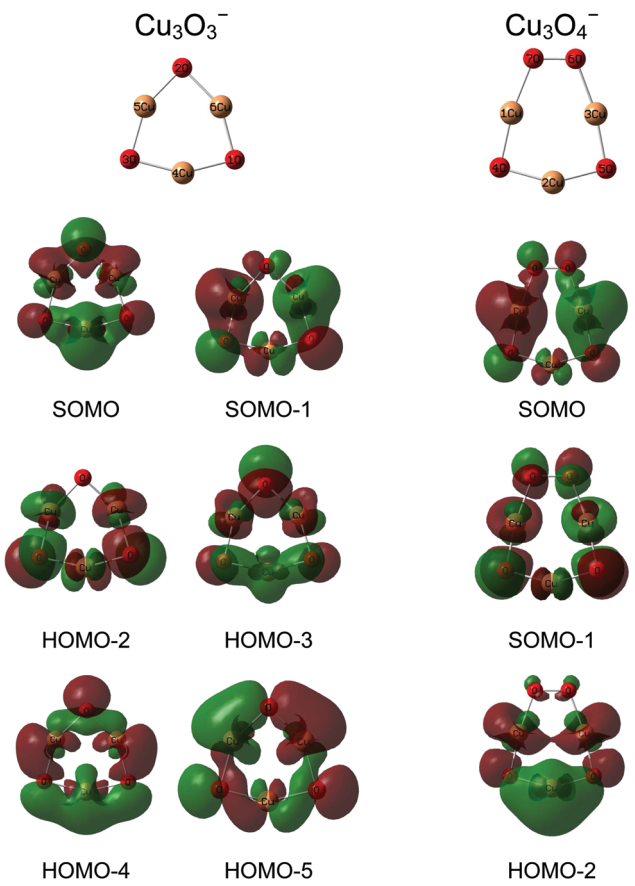

Fig. 4 Diagrams of the molecule orbitals of $Cu_3O_3^-$ and $Cu_3O_4^-$.

4. Conclusions

The $Cu_3O_3^-$ and $Cu_3O_4^-$ cluster anions were studied using mass-selected anion photoelectron spectroscopy and density functional theory calculations. The VDEs of $Cu_3O_3^-$ and $Cu_3O_4^-$ were measured to be 3.48 ± 0.08 and 3.54 ± 0.08 eV, respectively based on their photoelectron spectra. The most stable structures of $Cu_3O_3^-$ and $Cu_3O_4^-$ were determined by comparing the calculated VDEs and simulated spectra with experimental data. $Cu_3O_3^-$ has a C_{3v} symmetric six-membered cyclic structure with alternating Cu–O bonds. $Cu_3O_4^-$ has a C_s symmetric seven-membered ring configuration with one peroxo unit. The Cu–Cu interactions of the

$Cu_3O_3^-$ and $Cu_3O_4^-$ clusters are weak, which can be confirmed by the Cu–Cu distances, constant electronic charge densities, bond order and molecular orbitals analyses. The $Cu_3O_3^-$ and $Cu_3O_4^-$ clusters exhibit significant aromaticity.

Conflicts of interest

There are no conflicts of interest to declare.

Acknowledgements

This work is supported by the National Natural Science Foundation of China (Grant No. 21773255) and the Chinese Academy of Sciences (Grant No. QYZDB-SSW-SLH024). The theoretical calculations were conducted on the China Scientific Computing Grid (ScGrid) of the Supercomputing Center, Computer Network Information Center of the Chinese Academy of Sciences.

References

1 C. Yuan, H. B. Wu, Y. Xie and X. W. Lou, *Angew. Chem., Int. Ed.*, 2014, **53**, 1488–1504.
2 H. Su, S. Jaffer and H. Yu, *Energ. Storage Mater.*, 2016, **5**, 116–131.
3 A. Fernando, K. L. Weerawardene, N. V. Karimova and C. M. Aikens, *Chem. Rev.*, 2015, **115**, 6112–6216.
4 Y. Z. Jiang, M. J. Hu, D. Zhang, T. Z. Yuan, W. P. Sun, B. Xu and M. Yan, *Nano Energy*, 2014, **5**, 60–66.
5 C. E. Elwell, N. L. Gagnon, B. D. Neisen, D. Dhar, A. D. Spaeth, G. M. Yee and W. B. Tolman, *Chem. Rev.*, 2017, **117**, 2059–2107.
6 H. B. Wu and L.-S. Wang, *J. Chem. Phys.*, 1997, **107**, 8221–8228.
7 H. B. Wu and L.-S. Wang, *J. Phys. Chem. A*, 1998, **102**, 9129–9135.
8 H. B. Wu and L.-S. Wang, *J. Chem. Phys.*, 1998, **108**, 5310–5318.
9 H. B. Xu, X. Li, X. B. Wang, C. F. Ding and L.-S. Wang, *J. Chem. Phys.*, 1998, **109**, 449–458.
10 G. L. Gutsev, P. Jena, H.-J. Zhai and L.-S. Wang, *J. Chem. Phys.*, 2001, **115**, 7935–7944.
11 G. L. Gutsev, C. W. Bauschlicher, H.-J. Zhai and L.-S. Wang, *J. Chem. Phys.*, 2003, **119**, 11135–11145.
12 X. Huang, H.-J. Zhai, J. Li and L.-S. Wang, *J. Phys. Chem. A*, 2006, **110**, 85–92.
13 W.-J. Chen, H.-J. Zhai, Y. F. Zhang, X. Huang and L.-S. Wang, *J. Phys. Chem. A*, 2010, **114**, 5958–5966.
14 J. Y. Yuan, H.-G. Xu, X. Y. Kong and W. J. Zheng, *Chem. Phys. Lett.*, 2013, **564**, 6–10.
15 R.-Z. Li, J. Liang, X.-L. Xu, H.-G. Xu and W.-J. Zheng, *Chem. Phys. Lett.*, 2013, **575**, 12–17.
16 G. L. Gutsev, K. G. Belay, K. V. Bozhenko, L. G. Gutsev and B. R. Ramachandran, *Phys. Chem. Chem. Phys.*, 2016, **18**, 27858–27867.
17 O. Hubner and H. J. Himmel, *Angew. Chem., Int. Ed.*, 2017, **56**, 12340–12343.
18 W. L. Li, J. B. Lu, L. Zhao, R. Ponec, D. L. Cooper, J. Li and G. Frenking, *J. Phys. Chem. A*, 2018, **122**, 2816–2822.
19 H. J. Zhai, W. J. Chen, S. J. Lin, X. Huang and L. S. Wang, *J. Phys. Chem. A*, 2013, **117**, 1042–1052.
20 W. J. Qi, C. Z. Huang and L. Q. Chen, *Talanta*, 2010, **80**, 1400–1405.
21 L. M. Polak, M. K. Gilles, J. Ho and W. C. Lineberger, *J. Phys. Chem.*, 1991, **95**, 3460–3463.
22 H. B. Wu, S. R. Desai and L.-S. Wang, *J. Chem. Phys.*, 1995, **103**, 4363–4366.
23 H. B. Wu, S. R. Desai and L.-S. Wang, *J. Phys. Chem. A*, 1997, **101**, 2103–2111.
24 L.-S. Wang, H. B. Wu, S. R. Desai and L. Lou, *Phys. Rev. B: Condens. Matter Mater. Phys.*, 1996, **53**, 8028–8031.
25 Y. Gong and M. F. Zhou, *Phys. Chem. Chem. Phys.*, 2009, **11**, 8714–8720.
26 Y. Gong, G. J. Wang and M. F. Zhou, *J. Phys. Chem. A*, 2009, **113**, 5355–5359.
27 K. Deng, J. L. Yang and Q. S. Zhu, *J. Chem. Phys.*, 2000, **113**, 7867–7873.
28 Y. Pouillon and C. Massobrio, *Chem. Phys. Lett.*, 2002, **356**, 469–475.
29 C. Massobrio and Y. Pouillon, *J. Chem. Phys.*, 2003, **119**, 8305–8310.
30 Y. Pouillon and C. Massobrio, *Appl. Surf. Sci.*, 2004, **226**, 306–312.
31 T. Baruah, R. R. Zope and M. R. Pederson, *Phys. Rev. A: At., Mol., Opt. Phys.*, 2004, **69**, 023201.
32 B. Dai, L. Tian and J. L. Yang, *J. Chem. Phys.*, 2004, **120**, 2746–2751.
33 G. L. Gutsev, B. K. Rao and P. Jena, *J. Phys. Chem. A*, 2000, **104**, 11961–11971.
34 K. Pradhan, G. L. Gutsev, C. A. Weatherford and P. Jena, *J. Chem. Phys.*, 2011, **134**, 144305.
35 N. Orms and A. I. Krylov, *J. Phys. Chem. A*, 2018, **122**, 3653–3664.
36 G. T. Bae, B. Dellinger and R. W. Hall, *J. Phys. Chem. A*, 2011, **115**, 2087–2095.
37 G.-T. Bae, *Bull. Korean Chem. Soc.*, 2016, **37**, 638–642.
38 F. Yang, Q. Sun, L. L. Ma, Y. Jia, S. J. Luo, J. M. Liu, W. T. Geng, J. Y. Chen, S. Li and Y. Yu, *J. Phys. Chem. A*, 2010, **114**, 8417–8422.
39 M. Jadraque and M. Martín, *Chem. Phys. Lett.*, 2008, **456**, 51–54.
40 S. Hirabayashi and M. Ichihashi, *J. Phys. Chem. A*, 2018, **122**, 4801–4807.
41 S. Grundner, M. A. C. Markovits, G. N. Li, M. Tromp, E. A. Pidko, E. J. M. Hensen, A. Jentys, M. Sanchez-Sanchez and J. A. Lercher, *Nat. Commun.*, 2015, **6**, 7546.
42 K. D. Vogiatzis, G. N. Li, E. J. M. Hensen, L. Gagliardi and E. A. Pidko, *J. Phys. Chem. C*, 2017, **121**, 22295–22302.
43 G. Li, P. Vassilev, M. Sanchez-Sanchez, J. A. Lercher, E. J. M. Hensen and E. A. Pidko, *J. Catal.*, 2016, **338**, 305–312.

44 H.-G. Xu, Z.-G. Zhang, Y. Feng, J. Y. Yuan, Y. C. Zhao and W. J. Zheng, *Chem. Phys. Lett.*, 2010, **487**, 204–208.

45 C. Lee, W. Yang and R. G. Parr, *Phys. Rev. B: Condens. Matter Mater. Phys.*, 1988, **37**, 785–789.

46 A. D. Becke, *J. Chem. Phys.*, 1993, **98**, 5648–5652.

47 M. J. Frisch, G. W. Trucks, H. B. Schlegel, G. E. Scuseria, M. A. Robb, J. R. Cheeseman, G. Scalmani, V. Barone, B. Mennucci, G. A. Petersson, H. Nakatsuji, M. Caricato, X. Li, H. P. Hratchian, A. F. Izmaylov, J. Bloino, G. Zheng, J. L. Sonnenberg, M. Hada, M. Ehara, K. Toyota, R. Fukuda, J. Hasegawa, M. Ishida, T. Nakajima, Y. Honda, O. Kitao, H. Nakai, T. Vreven, J. J. A. Montgomery, J. E. Peralta, F. Ogliaro, M. Bearpark, J. J. Heyd, E. Brothers, K. N. Kudin, V. N. Staroverov, T. Keith, R. Kobayashi, J. Normand, K. Raghavachari, A. Rendell, J. C. Burant, S. S. Iyengar, J. Tomasi, M. Cossi, N. Rega, J. M. Millam, M. Klene, J. E. Knox, J. B. Cross, V. Bakken, C. Adamo, J. Jaramillo, R. Gomperts, R. E. Stratmann, O. Yazyev, A. J. Austin, R. Cammi, C. Pomelli, J. W. Ochterski, R. L. Martin, K. Morokuma, V. G. Zakrzewski, G. A. Voth, P. Salvador, J. J. Dannenberg, S. Dapprich, A. D. Daniels, O. Farkas, J. B. Foresman, J. V. Ortiz, J. Cioslowski and D. J. Fox, *Gaussian 09, Revision A. 02*, Gaussian, Inc., Wallingford, CT, 2009.

48 T. H. Dunning Jr., *J. Chem. Phys.*, 1989, **90**, 1007–1023.

49 K. A. Peterson, D. Figgen, M. Dolg and H. Stoll, *J. Chem. Phys.*, 2007, **126**, 124101.

50 S. Subramanian, R. Valantina and C. Ramanthan, *Mater. Sci.-Medzg.*, 2015, **21**, 173.

51 A. E. Reed, L. A. Curtiss and F. Weinhold, *Chem. Rev.*, 1988, **88**, 899–926.

52 T. Lu and F. Chen, *J. Comput. Chem.*, 2012, **33**, 580–592.

53 D. J. Tozer and N. C. Handy, *J. Chem. Phys.*, 1998, **109**, 10180–10189.

54 J. Akola, M. Manninen, H. Häkkinen, U. Landman, X. Li and L.-S. Wang, *Phys. Rev. B: Condens. Matter Mater. Phys.*, 1999, **60**, R11297–R11300.

55 K. Jug, B. Zimmermann, P. Calaminici and A. M. Köster, *J. Chem. Phys.*, 2002, **116**, 4497–4507.

56 H. J. Zhai, B. B. Averkiev, D. Y. Zubarev, L. S. Wang and A. I. Boldyrev, *Angew. Chem., Int. Ed.*, 2007, **46**, 4277–4280.

57 P. von Ragué Schleyer, C. Maerker, A. Dransfeld, H. J. Jiao and N. J. R. v. E. Hommes, *J. Am. Chem. Soc.*, 1996, **118**, 6317–6318.

58 Z. F. Chen, C. S. Wannere, C. Corminboeuf, R. Puchta and P. v. R. Schleyer, *Chem. Rev.*, 2005, **105**, 3842–3888.

59 H. Fallah-Bagher-Shaidaei, C. S. Wannere, C. Corminboeuf, R. Puchta and P. v. R. Schleyer, *Org. Lett.*, 2006, **8**, 863–866.

60 P. v. R. Schleyer, H. J. Jiao, N. J. R. v. E. Hommes, V. G. Malkin and O. L. Malkina, *J. Am. Chem. Soc.*, 1997, **119**, 12669–12670.

61 P. v. R. Schleyer, M. Manoharan, Z. X. Wang, B. Kiran, H. J. Jiao, R. Puchta and N. J. R. v. E. Hommes, *Org. Lett.*, 2001, **3**, 2465–2468.